Controlling Light Absorption in Charge-Separating Core/Shell Semiconductor Nanocrystals

Rekha Mahadevu, Aniruddha R. Yelameli, Bharati Panigrahy, and Anshu Pandey*

Solid State and Structural Chemistry Unit, Indian Institute of Science, Bangalore 560012, India

ABSTRACT Semiconductor nanocrystals of different formulations have been extensively studied for use in thin-film photovoltaics. Materials used in such devices need to satisfy the stringent requirement of having large absorption cross sections. Hence, type-II semiconductor nanocrystals that are generally considered to be poor light absorbers have largely been ignored. In this article, we show that type-II semiconductor nanocrystals can be tailored to match the light-absorption abilities of other types of nanostructures as well as bulk semiconductors. We synthesize type-II ZnTe/CdS core/shell nanocrystals. This material is found to exhibit a tunable band gap as well as absorption cross sections that are comparable to CdTe. This result has significant implications for thin-film photovoltaics, where the use of type-II nanocrystals instead of pure semiconductors can improve charge separation while also providing a much needed handle to regulate device composition.

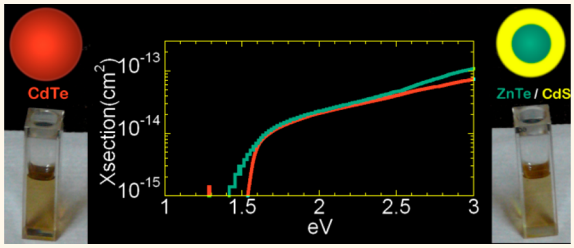

KEYWORDS: semiconductor nanocrystal · quantum dot · heterostructure · absorption cross section · type-II

Thin-film photovoltaics employ polycrystalline or amorphous materials to minimize fabrication costs. Semiconductors used to make such devices are associated with a large density of defects that are ultimately detrimental to device performance. The presence of a large number of defects in these materials thus makes device design a difficult conundrum. From the efficiency viewpoint, one would aim to minimize the number of defects by minimizing the amount of semiconductor used in such a device. From the stand point of maximizing current, one aims to create the thickest device possible to maximize the light absorbed. The light-absorption characteristics of a semiconductor thus play a central role in determining its suitability in a thin-film device.

Colloidal materials based on direct-gap semiconductors have been extensively investigated for use in these devices because of their large absorption cross sections and physical properties as well as their ease of synthesis. Nanocrystals synthesized from diverse materials such as PbSe,[1−5] PbS,[6] CdSe,[7−12] CdTe,[13−17] CIS,[18−20] FeS_2,[21] and others have been successfully used in devices. Most studies on colloidal materials have focused on pure semiconductors, alloys, as well as type-I core/shell structures; type-II materials have, in most[17] cases, been disregarded.

Type-II semiconductor nanocrystals (NCs) are materials where the band offsets of the two semiconductor layers are staggered so that after excitonic cooling, electrons and holes reside in different semiconductor layers.[22] The consequent reduction in the overlap of the electron and hole wave functions of the relaxed exciton gives rise to several unusual properties. Phenomena such as enhanced radiative lifetimes[23] as well as exciton−exciton repulsion[24] have been recently used to demonstrate NC lasers.[25]

The reduced electron−hole overlap that makes type-II NCs attractive for certain applications is one of the key reasons for the disinterest in type-II NC photovoltaics. The absorption cross section that is directly related to the electron−hole overlap is expected to be much weaker when compared to parent II−VI materials. Type-II-material-based devices are thus expected to be much thicker and therefore relatively inefficient when compared to other types of NC devices.

* Address correspondence to anshup@sscu.iisc.ernet.in.

Received for review September 10, 2013 and accepted November 19, 2013.

Published online November 19, 2013
10.1021/nn404749n

© 2013 American Chemical Society

In this article, we show that the absorption cross section of a type-II structure is not necessarily as low as the above reasoning would suggest. Rather, it may actually end up being comparable to or even higher than the cross sections of some single-component semiconductor materials that are being actively studied for photovoltaics.

Light absorption in a semiconductor material is dependent on its Kane parameter.[26,27] All II−VI semiconductors exhibit Kane parameter values that are roughly similar.[26] The differences between the light absorption of a single-component semiconductor and a core/shell structure therefore arise from other nonintrinsic effects that we aim to regulate and control in this work. To infer the relevance of various parameters in determining light absorption, it is useful to draw direct comparisons between the light-absorption characteristics of AX−BY heterojunctions and a single-component semiconductor, for example, AY or BX. Furthermore, of the two potential choices, AY and BX, it is most convenient to pick the semiconductor material with a band gap that is closest to the optical bandgap of the AX−BY heterojunction. For example, a ZnSe−CdS heterojunction with an optical band gap of 1.83 eV[22] can be readily compared to CdSe (band gap 1.75 eV) rather than to ZnS (band gap 3.91 eV).[28] This comparison is also motivated by the effective mass picture of these materials. In this formalism, the conduction band edge originates from cell periodic functions arising from the cation, whereas valence band is determined by the anion. In a type-II AX−BY structure where holes relax to the AX layer and electrons to the BY layer, the wave functions of carriers at the band edge are thus composed of lattice periodic function that are similar to the ones that make up the band edges of BX. This suggests a similarity in the properties of the seemingly unrelated AX−BY and BX semiconductors.

In this article, we primarily study the light-absorption characteristics of the solar-energy-relevant ZnTe/CdS heterostructure. Although both ZnTe and CdS have band gaps greater than 2 eV, the resultant type-II core/shell structure is expected from theory[29] to have an optical band gap comparable to the band gap of CdTe (1.45 eV).[28] With the Kane parameters of ZnTe, CdS, and CdTe being similar,[26] the primary differences in the absorption cross sections between ZnTe/CdS and CdTe arise from differences in carrier overlap as well as the density of states.

RESULTS AND DISCUSSION

ZnTe/CdS NCs were synthesized using colloidal techniques. Tellurium has an unusually low reduction potential among the chalcogenides that makes synthesis of telluride NCs and their core/shell structures particularly challenging. In view of the potential photovoltaic applications of this material, the use of the pyrophoric diethylzinc precursor was avoided during synthesis; instead, we used zinc chloride as the zinc precursor, whereas an alcoholic solution of sodium hydrogen telluride was employed as the tellurium precursor.

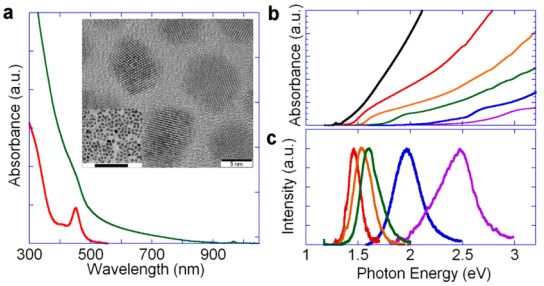

Figure 1. (a) Absorption spectrum of ZnTe (lower) and 9 nm diameter ZnTe/CdS NCs (offset). The inset shows TEM images of ZnTe/CdS NCs. Scale bars are 100 and 5 nm, respectively. (b) Absorption and (c) PL spectra of different samples of ZnTe/CdS.

Zinc telluride NCs are extremely susceptible to oxidation; we observed that these NCs can even be oxidized by organic sulfur solutions. The exposure of ZnTe NCs to a solution of sulfur in octadecene (a precursor commonly employed in the SILAR approach)[30] led to the appearance of a black precipitate. The composition of this precipitate was consistent with surface-oxidized aggregated NCs. The synthesis of the ZnTe/CdS NCs thus needed to rely upon a less oxidizing sulfur precursor where sulfur is preferably in a completely reduced (−II) state. We found that sulfide ions from metal salts such as sodium sulfide led to problems of independent nucleation. We therefore focused on obtaining a sulfur precursor that was not as oxidizing as elemental sulfur and not as reactive as an alkali metal sulfide. Primary amines are known to react with elemental sulfur to form polysulfides that gradually decompose to form hydrogen sulfide.[31] We found that these compounds do not appear to oxidize ZnTe NCs and at the same time react slowly enough to prevent the occurrence of independent nucleation.

In a typical synthesis, sodium hydrogen telluride was prepared by the reduction of elemental tellurium by sodium borohydride dissolved in diol (1,4-butanediol) under argon. The excess sodium borohydride was consumed by the addition of dextrose. In a second flask, a solution of zinc chloride in oleylamine and octadecene was heated at 150 °C. The solution of sodium hydrogen telluride was swiftly injected into the second flask to form ZnTe NCs. The temperature of the flask was then increased to 250 °C for CdS shell growth. Cadmium oleate and oleylamine polysulfide were used as precursors. A stock solution of polysulfide was prepared by heating elemental sulfur in oleylamine under an inert atmosphere. The precise details of the synthetic techniques are presented in the Materials and Methods section.

The as-synthesized ZnTe NCs have sharp spectral features; however, growth of an epitaxial CdS shell leads to smearing out of the optical spectrum along with the appearance of an absorption tail. In the example shown in Figure 1a, this new absorption band extends into the near-infrared until ∼900 nm.

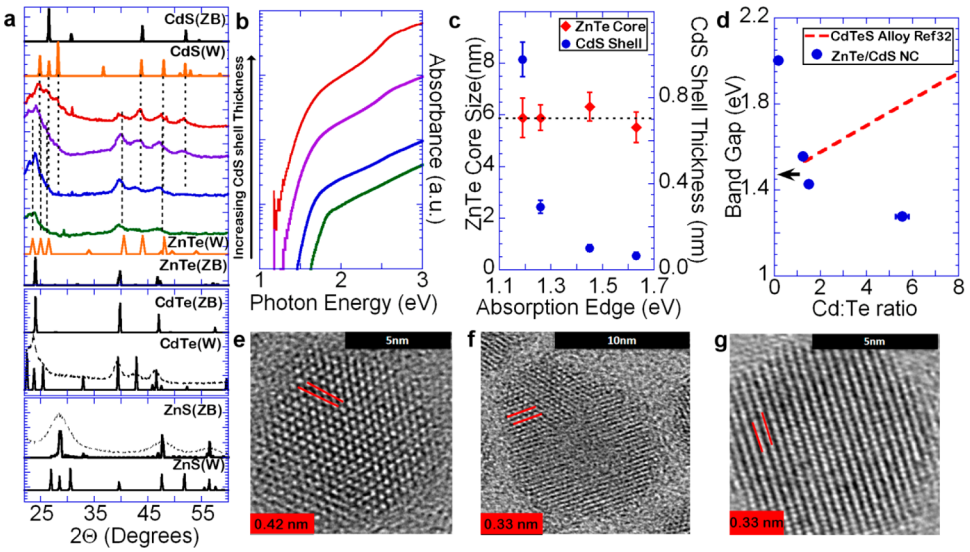

Figure 2. (a) Comparison of powder XRD pattern of ZnTe/CdS NCs with powder patterns of (from bottom to top) ZnS (Wurtzite, W; zinc blende, ZB), CdTe(W; ZB), ZnTe(ZB; W), and CdS(W; ZB). Powder patterns of CdTe and ZnS NCs (dashed lines) are also shown for comparison. As the CdS shell thickness increases on the ZnTe core, reflexes corresponding to CdS increase in amplitude. The four patterns correspond to four different stages of growth of CdS on ZnTe, with the lower (green) spectrum corresponding to the thinnest shell and the upper (red) spectrum corresponding to the thickest CdS shell. (b) Absorption spectra of the samples corresponding to XRD patterns of ZnTe/CdS. (c) ZnTe core size (left, diamonds) and CdS shell size (right, circles), as inferred from the XRD patterns shown in panel a, plotted against absorption edges inferred from panel b. (d) Evolution of the band gap of a batch of ZnTe/CdS NCs as the Cd/Te ratio increases because of CdS shell growth (blue solid circles). The dashed line is a linear fit to the variation of the band gap of a bulk CdTeS alloy as a function of the Cd/Te ratio, which is based on data presented in ref 32. The arrow represents the optical band gap of a bulk CdTe/CdS heterojunction, which is based on data in refs 28 and 29). (e) HRTEM image of a NC showing fringes with a 0.42 nm spacing corresponding to ZnTe. (f) HRTEM image of a NC showing fringes with a 0.33 nm spacing corresponding to CdS. (g) HRTEM image of a NC showing fringes with a 0.33 nm spacing corresponding to CdS.

The absorption and PL spectra of these NCs can be tuned across the visible to near-IR spectral region. In the data shown in Figure 1b,c, the tunability has been achieved by varying both the core diameter as well as the shell thickness. NCs with the largest ZnTe cores and the thickest CdS shells synthesized during the course of this work are found to exhibit a band gap as low as 1.18 eV. The NCs resulting from this synthesis are thus narrower gap materials than CdTe. In Figure 1b, the ZnTe core diameter is 5 nm for the four samples with the narrowest optical band gap. The two subsequent samples are derived from ZnTe cores that have diameters of 1 and 5 nm, respectively. The CdS shell thicknesses for samples in order of increasing optical band gap are 5, 2.8, 2.5, 2, 1, and 0.5 nm, respectively. Figure 2 illustrates the structural characteristics of the resulting material. The X-ray diffraction (XRD) patterns shown in Figure 2a are consistent with the formation of a ZnTe/CdS core/shell NC. For ZnTe/CdS (thin shell), the XRD patterns are ZnTe-like. Progressive addition of Cd and S precursors causes the optical band gap to red shift (Figure 2b) along with the emergence of reflexes corresponding to CdS in the XRD pattern in Figure 2a. Lines corresponding to secondary phases such as CdTe or ZnS are not observed at any stage. For the purpose of comparison, powder patterns of ZnTe, ZnS, CdS, CdTe have been included in this figure; broadened patterns observed in the case of NCs have also been included where possible. The clear emergence of reflexes corresponding to the shell semiconductor without the emergence of reflexes corresponding to impurity phases such as CdTe is indicative of the structural purity of the material.

Two significant features are noticeable in the X-ray diffraction patterns. First, we do not observe a shift of the pattern as a function of shell growth. A shift in the position of various reflexes as a function of the addition of shell precursors would be consistent with the formation of a macroscopic alloy. The absence of any such shift along with the presence of reflexes corresponding to ZnTe and CdS is consistent with the formation of a core/shell structure. Second, we observe that even though the reflexes corresponding to ZnTe diminish in amplitude their angular spread is unchanged as the CdS shell is grown. In terms of the Debye–Scherrer formula, this directly implies that the size of the ZnTe core does not change as the cadmium and sulfur precursors are added. In particular, we used the Scherrer equation to extract the sizes of the ZnTe core at various stages of shell growth. This is plotted in Figure 2c as a function of the nanocrystal absorption edge. This analysis shows that the starting size of the ZnTe core is 5.8 nm. This size remains unchanged during the course of the synthesis. In contrast, we

observe a clear narrowing of the reflexes corresponding to CdS, consistent with the growth of a CdS shell over the ZnTe core. The continuous increase in the size of the shell along with conservation of the size of the core is consistent with a core/shell structure. The data presented in Figure 2c can further be employed to determine the structure of the sample quantitatively. Given the errors associated with this analysis, we estimate that an interface alloy, if formed, can account for no more than 4% of the total NC volume.

Figure 2d illustrates the compositional characteristics of this material. The stoichiometry of samples is determined by inductively coupled plasma–optical emission spectroscopy (ICP–OES). A typical sample that exhibits a band gap of 1.3 eV is found to have a chemical formula $Zn_1Te_1Cd_{10}S_x$. For a core/shell structure, this would correspond to a 1:10 ratio of ZnTe/CdS. However, in principle, these elements could also be used to produce a variety of CdTe-based alloys and core/shells (*e.g.*, CdTeS/ZnS). We note that such structures have been studied extensively in the literature.[32,33] A CdTeS structure with a 10:1 cadmium-to-tellurium ratio is known to have a much higher band gap of 2.3 eV.[32,33] Figure 2d illustrates this effect for a single synthesis. Progressive addition of cadmium and sulfur precursors causes the composition of the NCs to change. With an increasing cadmium-to-tellurium ratio, the material band gap decreases. This behavior is unlike the well-known behavior of CdTeS alloys where the band gap increases with the increasing Cd/Te ratio. In Figure 2d, the behavior of bulk CdTeS alloys is depicted by the dashed line that is a fit to the data in ref 32. Over the composition range shown in the figure, the variation of band gap of CdTeS alloys with Cd/Te ratio is adequately described by a straight line fit. Figure 2d also shows the expected CdTe/CdS optical band gap for a bulk heterojunction (indicated by a black arrow symbol).[29] The NCs produced by our synthesis clearly have a much narrower band gap than what is associated with CdTe as well as its alloys and heterojunctions. It is thus possible to discount the role of CdTe or a CdTe alloy in determining the band edge optical properties of the material produced through our synthesis.

Finally, Figure 2e–g shows structural characteristics of this material at a single-particle level. HRTEM images of three representative QDs are shown in Figure 2e–g. All figures correspond to a ZnTe core size of 4.5 nm but different CdS shell thicknesses. Figure 2e corresponds to a 1.2 nm CdS shell, Figure 2f, to a 2.8 nm CdS shell, and Figure 2g, to a 2.3 nm CdS shell. The fringe spacing observed in the case of Figure 2e corresponds to the [220] planes of ZnTe, whereas the spacing observed in Figure 2f,g corresponds to the [002] plane of CdS.[34] The clear correspondence between the HRTEM and the XRD patterns suggests that the NCs are phase pure; CdZnTeS alloys and/or phases of CdTe or ZnS are undetectable both at an ensemble as well as at a single-particle level.

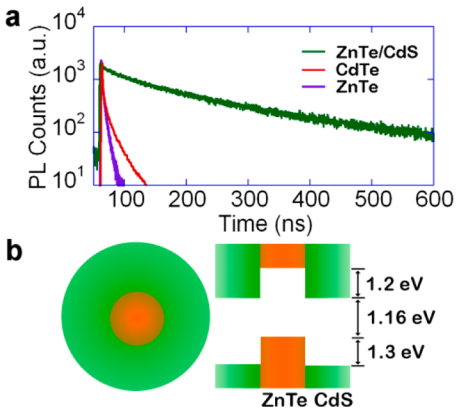

Figure 3. (a) Like other type-II NCs, ZnTe/CdS NCs exhibit somewhat longer exciton decay lifetimes compared to pure semiconductor NCs, CdTe and ZnTe. (b) Band offset of ZnTe/CdS NCs as inferred from this work.

Structurally, we are therefore able to eliminate completely the possibility of the presence of a large amount of CdTe or a CdTe alloy in our samples. An interface alloy, if present, can account for no more than 4% of the total nanocrystal volume. An extrinsic property, such as absorption cross sections, would thus be unaffected by the presence of such a small amount of a secondary phase. To summarize, the NCs synthesized here have no structural, physical, or spectroscopic resemblance to CdTe-based alloys and core shells. We thus unambiguously consider these materials to be ZnTe/CdS NCs in the remainder of this article.

Other characteristics of these NCs are also typical of the properties expected from type-II heterostructures. Most notably, these NCs exhibit a much longer exciton recombination lifetime than single-component NCs. Figure 3a compares the PL decay kinetics of one such sample with the decay kinetics of CdTe NCs. Both NCs have identical PL quantum yields (8%) and similar emission wavelengths (630 nm for ZnTe/CdS and 626 nm for CdTe). The biexponential exciton decay (70%, 3 ns and 30%, 24 ns) that is observed in the CdTe NC sample shown here is fairly typical of a single-component II–VI material where the exciton fine structure leads to an emission rate that is marginally slower than what is expected from the band edge absorption cross section. The behavior of a ZnTe NC is also seen to be similar (50%, 2 ns and 50%, 9 ns). In a type-II material such as ZnTe/CdS, the separation of electrons and holes leads to a significant reduction in carrier–carrier overlap and consequently the exciton recombination rate (45%, 40 ns and 55%, 200 ns). The long exciton lifetimes in these materials are potentially advantageous for light harvesting because this would provide any working device a greater amount of time to separate charges.

The k.p method may be employed to fit the absorption band edges of various samples. We employ a model[22,35] with a nonparabolic conduction band. Band

edge electron effective mass are taken to be 0.21 and 0.2 in CdS and ZnTe, respectively, whereas 0.8 and 0.2 are taken to be the masses of heavy holes in the two materials, respectively.[28] Under this model,[22,28,36] our data can be reasonably fit by a 1.2 eV conduction band offset between ZnTe and CdS. The choice of this offset implies that ZnTe/CdS heterojunctions could, in principle, exhibit an optical band gap as low as 1.16 eV. From a band gap point of view, these NCs are thus well-suited for photovoltaics.[37]

The above survey of physical, structural, and optical characteristics of ZnTe/CdS NCs suggests that the NCs are excellent photovoltaic materials in many ways. The effective optical band gap is close to the Shockley–Quiesser optimum of 1.1 eV,[37] the carrier lifetimes are much longer than in single-component materials, and, finally, the NCs themselves are air-stable. The only outstanding issue is their optical absorption characteristics, which we will turn to in the discussion below.

The most striking characteristic of these NCs is the absorption tail that extends well below the band gaps of either constituent semiconductor (2.39 eV for ZnTe and 2.50 eV for CdS).[28] For purposes of light harvesting, this absorption tail is thus of primary relevance because it enables ZnTe/CdS NCs to absorb across a significantly greater solar spectral window.

In light of the above practical considerations, we divide interband transitions in type-II NCs into two rather arbitrary classes. For photons with energies higher than the band gap of either material, the electronic transition can potentially involve states delocalized over the entire structure. These transitions are labeled H in the inset of Figure 4. For photons with energies lower than the band gap of either material, the transition necessarily involves states that are localized into different semiconductor layers. These transitions are labeled L in the inset of Figure 4. This classification, although natural, is nevertheless arbitrary because envelope functions of both carriers do tunnel into the adjacent semiconductor layer.

The strength of light absorption is dependent on the transition dipole as well as the density of final states. States in the absorption tail have a low transition dipole moment that is also evidenced in the long exciton lifetimes in these materials. This concern may be recast into a more experimentally tangible form by considering the oscillator strengths of the two classes of transitions that we have indicated above. For simplicity, we consider all possible transitions of an electron that is initially located at the valence band edge of ZnTe. This is depicted in the inset of Figure 4.

Progressive increase in the thickness of the CdS shell has two effects. It increases the total volume of the NC, leading to increased total light absorption at all energies above the band gap. The second effect, more relevant to our discussion here, is a redistribution of oscillator strengths between the H and L transitions.

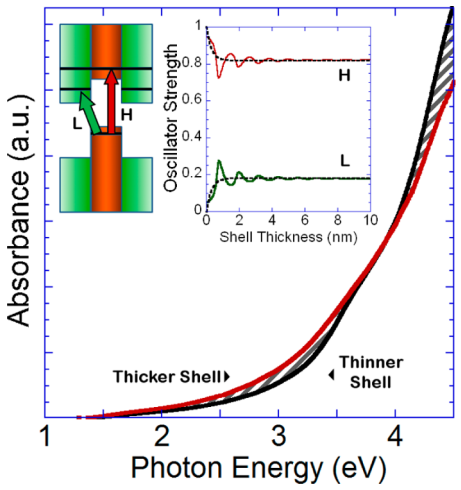

Figure 4. Changes in the absorption spectrum of ZnTe/CdS induced by a small increase in CdS shell thickness. The red (black) curve indicates the spectrum after (before) shell growth. The total area under each curve is constant. The shaded areas roughly correspond to spectral regions where the oscillator strengths are redistributed because of the small change in shell thickness. The inset shows the estimated changes in oscillator strength of transitions from the band edge s-like hole state. The upper (lower) curve, labeled H (L), corresponds to transitions occurring to conduction band levels with energies higher (lower) than the ZnTe conduction band edge. These transitions are also indicated in the schematic. Dashed lines are a guide to the eye.

As the CdS shell is grown on ZnTe, the conduction band levels located at the ZnTe band edge become increasingly bulk-like, whereas the band edge hole wave functions are relatively unchanged. The diffuse nature of the electron and the compact nature of the hole wave functions lead to a fall in the oscillator strengths of H transitions. In accordance with the sum rule of oscillator strengths, the oscillator strength lost from the H transitions is in turn transferred into the L transitions so that the total oscillator strength is conserved. The lower-energy transition thus borrows its oscillator strength from higher-energy transitions. Figure 4 shows the changes that result from the additional growth of CdS on a ZnTe/CdS(thin shell) NC. Besides the expected red shift of the band edge, additional CdS growth also causes the optical absorption at higher energies to diminish relative to the absorption at lower energies. To highlight this effect, both spectra have been normalized so that the area under each curve is constant. For samples with similar absorption cross sections, this is a reflection of the sum rule for oscillator strengths. The inset of Figure 4 shows an estimate of the degree of redistribution as the shell of CdS grows thicker. Increasing CdS shell thickness can thus lead to a transfer of ~20% of the oscillator strength of the H levels to the L levels. The magnitude of this transfer is a direct outcome of the large surface-to-volume ratio of colloidal NCs; other geometries have been shown to exhibit a substantially smaller redistribution.[38,39] Although the redistribution is substantial, all parameters

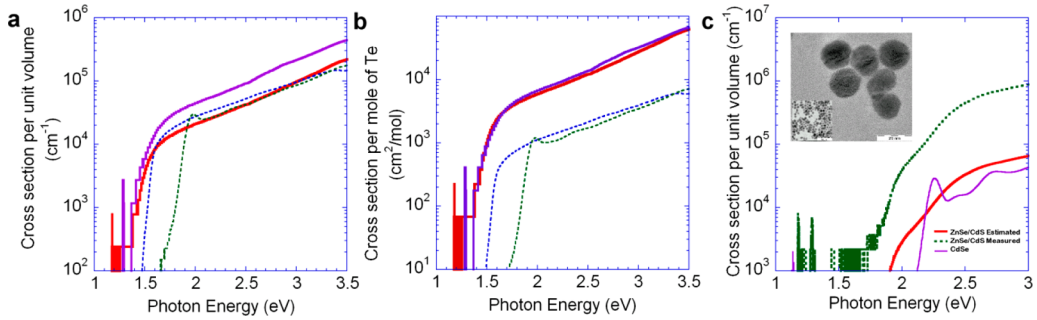

Figure 5. (a) Absorption cross sections per unit NC volume of ZnTe/CdS (solid lines) and CdTe (dashed lines) NCs dispersed in toluene. (b) Absorption cross sections of both sets of NCs normalized to the Te content. (c) Absorption cross sections per unit NC volume of ZnSe/CdS (dashed line, measured; solid line, estimated) and CdSe NCs.

remaining the same, the band edge of a type-II material would only be one-fifth as absorbing as the band edge of a regular single-component semiconductor. Fortunately, oscillator strength is only one of the determining factors, with the density of carrier states being the other key parameter. CdS has a conduction band effective mass that is twice as high as the conduction band effective mass of CdTe (0.21 for CdS, 0.11 for CdTe);[28] this directly implies a 2-fold higher conduction band density of states. A second important modification to the density of states is introduced by the different bulk band gaps of the materials. Since ZnTe/CdS (1.16 eV) has a lower effective band gap than CdTe (1.45 eV), at any particular photon energy it has a higher density of state. A rough estimate of the same can be obtained by considering a $(E - E_g)^{1/2}$ type dispersion. Here E is the photon energy and E_g is the semiconductor band gap. This contributes a factor of 3 at ~1.5 eV and a factor of 1.25 at 2 eV. Thus, the density of states in a ZnTe/CdS structure is between 6 to 2.5 times the density of states in CdTe over the 1.5−2 eV energy window. Even with only 20% of the integrated oscillator strength of the transitions occurring within the tail, this simple estimate suggests that optimal ZnTe/CdS NCs could in fact be 1.2 times more absorptive than CdTe in the 1.5 eV region.

This is an unexpected result; a judiciously designed type-II structure can thus be a better light absorber than a single-component semiconductor. This result is also surprising from the carrier lifetime point of view; type-II structures are associated with much longer carrier lifetimes, yet, as reasoned above, they can be stronger absorbers of light as well. This apparent paradox can be quite easily resolved: type-II structures always have a much weaker interband transition dipole but can be engineered to have a high density of states. During absorption, a valence band electron is promoted to an empty conduction band. The higher density of states can thus be used to compensate for the weaker transition dipole during light absorption. During emission, a conduction band electron falls into a single available valence band hole. The weaker transition dipole thus ensures a much slower recombination rate.

A direct measurement of the absorption cross section reveals that ZnTe/CdS is indeed roughly as absorptive as CdTe. Figure 5a compares the NC-volume-normalized absorption cross sections of type-II ZnTe/CdS NCs with those of CdTe NCs. Because ZnTe/CdS NCs exhibit nearly similar cross sections per unit volume to CdTe and have the additional advantage of much higher exciton lifetimes, photovoltaic devices based on these materials can, in principle, outperform their CdTe-based counterparts. The ZnTe/CdS NCs shown in Figure 5b have diameters of 10.5 and 16 nm, respectively, whereas the CdTe NCs have diameters 11 and 4 nm. The NCs typically have a 10% size dispersion; for example, for the 10.5 nm ZnTe/CdS NCs, we measure a 1.0 nm size dispersion. The cross sections per unit volume are not affected by ensemble polydispersity because this quantity has no explicit volume dependence. Errors in these measurements arise from instrument sensitivity issues and are expected to be within 1% of the measured result.

The substitution of single-component semiconductors with type-II materials has other advantages as well. As shown in Figure 5b, the NCs considered here have only one-tenth of the tellurium content of a typical CdTe NC. Given the 10% size dispersion in ensembles, of these NCs, a 30% variance is expected from NC to NC. By constructing type-II NCs out of electron- and hole-transporting semiconductors, it is possible to create NCs that preferentially support electron or hole transport. As shown in Figure 5b, the regulation of NC composition can be achieved without significantly affecting light absorption. The use of type-II NCs could thus allow for the manipulation of electron- and hole-flow directions in the absorbing layer itself, thereby leading to thinner, more efficient devices.

The cross sections in Figure 5a have been measured by determining the number of NCs in a solution by elemental analysis. In some cases, a rough estimate of the cross sections may also be made from bulk refractive indices.[40] The cross section of the type-II NC at high photon energies can be approximated by the absorption cross section of a QD made purely from the major component of the type-II NC.[41] In this approximation, one considers the absorption spectrum of a 10 nm ZnTe/CdS (thick shell) NC to be the same as the absorption of a 10 nm CdS QD at photon energies

much higher than the CdS band gap. The absorption cross section at lower energies is then inferred by normalizing the absorption spectrum. For samples with thick CdS shells, one thus assumes the absorption cross section to be $6.76 \times 10^{-16}\ a^3\ \mathrm{cm}^2$ at 4 eV. Here, a is the particle radius in nm. The results from this approximate procedure are very similar to the results obtained from a direct measurement. We note at this point that the results obtained so far are fairly general; any AX—BY type-II structure can have a higher absorption cross section than a single-component semiconductor AY provided the major component of the AX—BY heterostructure has a sufficiently high density of state. As yet another example, we measure the optical cross sections of ZnSe/CdS and find these to be similar to CdSe. This result is shown in Figure 5c.

CONCLUSIONS

We demonstrate that type-II semiconductor nanocrystals are spectroscopically better suited for thin-film photovoltaic devices than their single-component counterparts. The primary advantage offered by these materials is that they can absorb light just as well as a single-component direct gap semiconductor while exhibiting carrier lifetimes that can even be over an order of magnitude longer. Type-II NCs are thus extremely flexible materials where various properties such as absorption cross sections, emission lifetimes, and so forth can be controlled by regulating shell thickness. On the basis of considerations of their spectroscopic characteristics alone, devices made from type-II NCs should outperform devices based on single-component materials.

MATERIALS AND METHODS

Synthetic Methods. Tellurium (Te, 99.99%), zinc chloride ($ZnCl_2$, anhydrous 99.999%), sodium borohydride ($NaBH_4$ 96%), trioctylphosphine (TOP, technical grade, 90%), 1-octadecene (ODE, technical grade, 90%), oleylamine (technical grade, 70%), sulfur (S, <99.5%), and cadmium oxide (99.9%) were purchased from Sigma-Aldrich. 1,4-Butanediol (90%, AR) and dextrose (95% anhydrous, AR) were purchased from SD Fine Chemicals. All chemicals were used without further purification.

Zinc Telluride (ZnTe) Nanoparticle Synthesis. This synthesis involves two steps: initial preparation of sodium hydrogen telluride followed by the synthesis of ZnTe.Flask 1. Tellurium powder (0.1 mmol, 12.76 mg) and sodium borohydride ($NaBH_4$ 0.1 mmol, 9.45 mg) was added to a 50 mL three-necked flask containing 1 mL of diol (*i.e.*, 1,4-butanediol). This flask was heated at 60 °C under an argon atmosphere for about 15 min. $NaBH_4$ reduces elemental tellurium (Te(0)) to its Te(−II) state. Dextrose (0.1 mmol in 1 mL of 1,4-butanediol) was added to consume the excess borohydride. This step is important because the rapid injection of an unreacted borohydride solution into a heated flask (see step 2) may lead to a sudden release of hydrogen gas and an unexpected rise in pressure. TOP (0.2 mL) is then added.Flask 2. $ZnCl_2$ (0.1 mmol, 13.63 mg) was added to a separate flask (flask 2) containing ODE (4 mL, from Aldrich) as solvent and oleylamine (1 mL) as ligand. The mixture was degassed thoroughly and heated at 150 °C under an argon atmosphere. The contents of flask 1 were swiftly injected into flask 2.

CdS Shell Growth on ZnTe Quantum Dots. We observed that elemental S dissolved in ODE can oxidize ZnTe NCs, and this precluded the straightforward use of S/ODE as the sulfur precursor. The sulfur precursor (SP) was prepared by heating 32 mg of S powder in 5 mL of oleylamine at 250 °C for 5 min under an argon atmosphere. The resultant reddish solution was diluted with 5 mL of ODE. The cadmium precursor (CP), cadmium oleate, was separately prepared by heating 128 mg of cadmium oxide in oleic acid (3 mL) and octadecene (7 mL) at 300 °C for 10 min under argon. The resultant colorless solution was then degassed under vacuum for 5 min at 100 °C.

To grow ZnTe/CdS core/shell NCs, as-prepared ZnTe NCs were heated at 250 °C. SP and CP were added dropwise alternately (2 mL of each per hour) until the desired shell thickness was achieved. CdS shells were grown on ZnSe cores by employing a more conventional approach, with a 0.1 M solution of sulfur in octadecene as the sulfur precursor and 0.1 M cadmium oleate as the cadmium precursor. The reaction was conducted at 220 °C under an argon atmosphere, with the ZnSe NCs dispersed in 4 mL of octadecene and 1 mL of oleylamine.

The NCs were cleaned thoroughly after synthesis, before proceeding to analysis and characterization. Care was taken to remove excess ligands, solvents, and unreacted precursors. Cleaning of NCs involved three steps. Initially, 5 mL of methanol and 0.5 mL of ethanol were added to 5 mL of synthesized NCs, and the mixture was centrifuged for 1 min at 900 RCF (relative centrifugal force). This led to the formation of two immiscible layers. The upper layer, which contained dissolved reaction byproducts and unreacted chemicals in ethanol, was separated from the lower layer, which contained NCs dissolved in octadecene. The lower layer was used for the second step of purification. In the second step, 0.5 mL of methanol and 5 mL of ethanol were added and kept for centrifugation for 1 min at 900 RCF. For the third step, the lower layer was retrieved again, and 0.5 mL of methanol, 0.5 mL of ethanol, and 2 mL of isopropanol were added and kept for centrifugation for 1 min at 900 RCF. The supernatant was removed, and the NCs in were found precipitated in the form of a solid that adhered to the sides and the bottom of the tube. For spectroscopic studies, the NCs were typically dissolved in spectroscopic grade hexane or spectroscopic grade toluene and then centrifuged at 3600 RCF for 5 min. NC aggregates and insoluble byproducts were thereby precipitated. The supernatant was used for further studies. Spectroscopic data were collected with the NCs in either hexane or toluene solution.

XRD Patterns and Analysis. Films for XRD measurements were prepared by casting NCs from hexane solutions onto a glass substrate. A 0.154 nm source was used to collect all data. The core size was determined by applying the Scherrer equation to the reflex at 40.5°. The shape factor was taken to be 0.94 in all cases. The shell thickness was determined from the reflex at 51.8° using the knowledge of the core size.

Quantum Yield Measurements. Absolute quantum yields were determined using an integrating sphere. Samples were dissolved in hexane and introduced into the sphere in a quartz cuvette. The absorption of light at the excitation wavelength was determined by comparing with a reference cuvette with hexane.

Cross Section Measurements. Absorption cross section measurements were performed by first dissolving samples in toluene to take absorption spectra. The solvent was then evaporated, and the NCs were digested in concentrated HNO_3. The resultant solution was diluted to 25 mL. Composition was then determined using inductively coupled plasma. Size distributions were estimated from TEM images. The density of NCs was assumed to be identical to bulk CdS (4.82 g/cm^3). Quantum dots used in this work are typically less than 15 nm in size. Particles of this size do not scatter perceptibly. Extinction and absorption have thus been taken to be equal throughout this article.

Calculations. Effective mass calculations were performed using a Bastard model. The valence band was assumed to have a parabolic dispersion. The band offsets described in Figure 3

were obtained by fitting the spectral position of the S-exciton of the starting ZnTe NC and the end of the absorption tail of the type-II structure by the above model. The oscillator strengths described in Figure 4 were obtained by summing over the squares of overlap integrals between conduction and valence states. Aside from the usual approximations contained within k.p theory, this approximation also neglects differences in Kane velocities in the two materials (19.1 and 21 eV for ZnTe and CdS, respectively). A Lorentzian line width of 0.1 eV was assumed for each transition. The oscillations that are observed in Figure 4 (inset) are an outcome of this choice of line width; these are not expected to be observed in a real sample where valence band levels arising from hole states other than the 1S heavy hole would also contribute to optical absorption.

Conflict of Interest: The authors declare no competing financial interest.

Supporting Information Available: Supporting information available: Cross sections of ZnTe/CdS and CdTe samples, linear scale plot of absorption versus photon energy for ZnTe/CdS NCs with different CdS shell thickness, measured and estimated cross sections of ZnTe/CdS NCs, absorption cross sections per unit NC volume of ZnTe/CdS (Solid lines) and CdTe (Dashed lines) NCs dispersed in toluene, and HRTEM images of ZnTe/CdS core shell NCs showing different fringe spacings. This material is available free of charge *via* the Internet at http://pubs.acs.org.

Acknowledgment. We acknowledge funding from ISRO-IISc-STC through project code ISTC/CSS/AP/312. AP would like to acknowledge the Indian Institute of Science for generous start-up funding as well as Prof. D. D. Sarma for stimulating discussions.

REFERENCES AND NOTES

1. Hyun, B. R.; Bartnik, A. C.; Sun, L. F.; Hanrath, T.; Wise, F. W. Control of Electron Transfer from Lead-Salt Nanocrystals to TiO_2. *Nano Lett.* **2011**, *11*, 2126–2132.
2. Choi, J. J.; Lim, Y. F.; Santiago-Berrios, M. B.; Oh, M.; Hyun, B. R.; Sung, L. F.; Bartnik, A. C.; Goedhart, A.; Malliaras, G. G.; Abruna, H. D.; *et al.* PbSe Nanocrystal Excitonic Solar Cells. *Nano Lett.* **2009**, *9*, 3749–3755.
3. Choi, J. J.; Luria, J.; Hyun, B. R.; Bartnik, A. C.; Sun, L. F.; Lim, Y. F.; Marohn, J. A.; Wise, F. W.; Hanrath, T. Photogenerated Exciton Dissociation in Highly Coupled Lead Salt Nanocrystal Assemblies. *Nano Lett.* **2010**, *10*, 1805–1811.
4. Tisdale, W. A.; Williams, K. J.; Timp, B. A.; Norris, D. J.; Aydil, E. S.; Zhu, X. Y. Hot-Electron Transfer from Semiconductor Nanocrystals. *Science* **2010**, *328*, 1543–1547.
5. Leschkies, K. S.; Beatty, T. J.; Kang, M. S.; Norris, D. J.; Aydil, E. S. Solar Cells Based on Junctions between Colloidal PbSe Nanocrystals and Thin ZnO Films. *ACS Nano* **2009**, *3*, 3638–3648.
6. Zhitomirsky, D.; Furukawa, M.; Tang, J.; Stadler, P.; Hoogland, S.; Voznyy, O.; Liu, H.; Sargent, E. H. N-Type Colloidal-Quantum-Dot Solids for Photovoltaics. *Adv. Mater.* **2012**, *24*, 6181–6185.
7. Chanyawadee, S.; Harley, R. T.; Henini, M.; Talapin, D. V.; Lagoudakis, P. G. Photocurrent Enhancement in Hybrid Nanocrystal Quantum-Dot P-I-N Photovoltaic Devices. *Phys. Rev. Lett.* **2009**, *102*, 077402-1–077402-4.
8. Talgorn, E.; Abellon, R. D.; Kooyman, P. J.; Piris, J.; Savenije, T. J.; Goossens, A.; Houtepen, A. J.; Siebbeles, L. D. A. Supercrystals of CdSe Quantum Dots with High Charge Mobility and Efficient Electron Transfer to TiO2. *ACS Nano* **2010**, *4*, 1723–1731.
9. Loef, R.; Houtepen, A. J.; Talgorn, E.; Schoonman, J.; Goossens, A. Study of Electronic Defects in CdSe Quantum Dots and Their Involvement in Quantum Dot Solar Cells. *Nano Lett.* **2009**, *9*, 856–859.
10. Leschkies, K. S.; Divakar, R.; Basu, J.; Enache-Pommer, E.; Boercker, J. E.; Carter, C. B.; Kortshagen, U. R.; Norris, D. J.; Aydil, E. S. Photosensitization of ZnO Nanowires with CdSe Quantum Dots for Photovoltaic Devices. *Nano Lett.* **2007**, *7*, 1793–1798.
11. Robel, I.; Subramanian, V.; Kuno, M.; Kamat, P. V. Quantum Dot Solar Cells. Harvesting Light Energy with CdSe Nanocrystals Molecularly Linked to Mesoscopic TiO_2 Films. *J. Am. Chem. Soc.* **2006**, *128*, 2385–2393.
12. Yu, Y. H.; Kamat, P. V.; Kuno, M.; CdSe Nanowire/Quantum, A. Dot Hybrid Architecture for Improving Solar Cell Performance. *Adv. Funct. Mater.* **2010**, *20*, 1464–1472.
13. Jasieniak, J.; MacDonald, B. I.; Watkins, S. E.; Mulvaney, P. Solution-Processed Sintered Nanocrystal Solar Cells *via* Layer-by-Layer Assembly. *Nano Lett.* **2011**, *11*, 2856–2864.
14. MacDonald, B. I.; Martucci, A.; Rubanov, S.; Watkins, S. E.; Mulvaney, P.; Jasieniak, J. J. Layer-by-Layer Assembly of Sintered $CdSe_xTe_{1-x}$ Nanocrystal Solar Cells. *ACS Nano* **2012**, *6*, 5995–6004.
15. Zhu, H. M.; Song, N. H.; Lian, T. Q. Wave Function Engineering for Ultrafast Charge Separation and Slow Charge Recombination in Type II Core/Shell Quantum Dots. *J. Am. Chem. Soc.* **2011**, *133*, 8762–8771.
16. McDaniel, H.; Pelton, M.; Oh, N.; Shim, M. Effects of Lattice Strain and Band Offset on Electron Transfer Rates in Type-II Nanorod Heterostructures. *J. Phys. Chem. Lett.* **2012**, *3*, 1094–1098.
17. Shim, M.; McDaniel, H.; Oh, N. Prospects for Strained Type-II Nanorod Heterostructures. *J. Phys. Chem. Lett.* **2011**, *2*, 2722–2727.
18. Li, L.; Pandey, A.; Werder, D. J.; Khanal, B. P.; Pietryga, J. M.; Klimov, V. I. Efficient Synthesis of Highly Luminescent Copper Indium Sulfide-Based Core/Shell Nanocrystals with Surprisingly Long-Lived Emission. *J. Am. Chem. Soc.* **2011**, *133*, 1176–1179.
19. Li, L.; Coates, N.; Moses, D. Solution-Processed Inorganic Solar Cell Based on *in Situ* Synthesis and Film Deposition of $CuInS_2$ Nanocrystals. *J. Am. Chem. Soc.* **2010**, *132*, 22–23.
20. Jiang, C. Y.; Lee, J. S.; Talapin, D. V. Soluble Precursors for $CuInSe_2$, $CuIn_{(1-x)}Ga_{(x)}Se_{(2)}$, and $Cu_2ZnSn(S,Se)_{(4)}$ Based on Colloidal Nanocrystals and Molecular Metal Chalcogenide Surface Ligands. *J. Am. Chem. Soc.* **2012**, *134*, 5010–5013.
21. Puthussery, J.; Seefeld, S.; Berry, N.; Gibbs, M.; Law, M. Colloidal Iron Pyrite (FeS_2) Nanocrystal Inks for Thin-Film Photovoltaics. *J. Am. Chem. Soc.* **2011**, *133*, 716–719.
22. Pandey, A.; Guyot-Sionnest, P. Intraband Spectroscopy and Band Offsets of Colloidal II-VI Core/Shell Structures. *J. Chem. Phys.* **2007**, *127*, 104710-1–104710-10.
23. Kim, S.; Fisher, B.; Eisler, H. J.; Bawendi, M. Type-II Quantum Dots: CdTe/CdSe(Core/Shell) and CdSe/ZnTe(Core/Shell) Heterostructures. *J. Am. Chem. Soc.* **2003**, *125*, 11466–11467.
24. Klimov, V. I.; Ivanov, S. A.; Nanda, J.; Achermann, M.; Bezel, I.; McGuire, J. A.; Piryatinski, A. Single-Exciton Optical Gain in Semiconductor Nanocrystals. *Nature* **2007**, *447*, 441–446.
25. Dang, C.; Lee, J.; Breen, C.; Steckel, J. S.; Coe-Sullivan, S.; Nurmikko, A. Red Green and Blue Lasing Enabled by Single-Exciton Gain in Colloidal Quantum Dot Films. *Nat. Nanotechnol.* **2012**, *7*, 335–339.
26. Lawaetz, P. Valence-Band Parameters in Cubic Semiconductors. *Phys. Rev. B* **1971**, *4*, 3460–3467.
27. Khurgin, J. Comparative Analysis of the Intersubband *versus* Band-to-Band Transitions in Quantum Wells. *Appl. Phys. Lett.* **1993**, *62*, 1390–1392.
28. *Springer Handbook of Electronic and Photonic Materials*; Kasap, S., Capper, P., Eds.; Springer: New York, 2007.
29. Wei, S. H.; Zunger, A. Calculated Natural Band Offsets of All II-VI and III-V Semiconductors: Chemical Trends and the Role of Cation d Orbitals. *Appl. Phys. Lett.* **1998**, *72*, 2011–2013.
30. Li, J. J.; Wang, Y. A.; Guo, W. Z.; Keay, J. C.; Mishima, T. D.; Johnson, M. B.; Peng, X. G. Large-Scale Synthesis of Nearly Monodisperse CdSe/CdS Core/Shell Nanocrystals Using Air-Stable Reagents *via* Successive Ion Layer Adsorption and Reaction. *J. Am. Chem. Soc.* **2003**, *125*, 12567–12575.
31. Davis, R. E.; Nakshbendi, H. F. Sulfur in Amine Solvents. *J. Am. Chem. Soc.* **1962**, *84*, 2085–2090.
32. Wei, K.; Pollak, F. H.; Freeouf, J. L.; Shvydka, D.; Compaan, A. D. Optical Properties of $CdTe_{(1-x)}S_{(x)}$ ($0 \leq x \leq 1$): Experiment and Modeling. *J. Appl. Phys.* **1999**, *85*, 7418–7425.
33. Tang, Z.; Wang, Y.; Shanbhag, S.; Kotov, N. A. Spontaneous CdTe Alloy−CdS Transition of Stabilizer-Depleted CdTe Nanoparticles Induced by EDTA. *J. Am. Chem. Soc.* **2006**, *128*, 7036–7042.

34. Li, Z.; Cai, W.; Sui, J. Large-Scale Preparation of CdS Quantum Dots by Direct Thermolysis of a Single-Source Precursor. *Nanotechnology* **2008**, *19*, 035602.
35. Bastard, G.; Brum, J. A. Electronic States in Semiconductor Heterostructures. *IEEE J. Quantum Electron.* **1986**, *22*, 1625–1644.
36. Venghaus, H.; Jusserand, B.; Behnke, G. Valence Band Parameters and Free Exciton Reduced Mass of Zinc Telluride Derived from Free Exciton Magnetoreflectance. *Solid State Commun.* **1980**, *33*, 371–375.
37. Shockley, W.; Queisser, H. J. Detailed Balance Limit of Efficiency of P-N Junction Solar Cells. *J. Appl. Phys.* **1961**, *32*, 510–519.
38. Schrier, J.; Demchenko, D. O.; Wang, L. W.; Alivisatos, A. P. Optical Properties of ZnO/ZnS and ZnO/ZnTe Heterostructures for Photovoltaic Applications. *Nano Lett.* **2007**, *7*, 2377–2382.
39. Giblin, J.; Kuno, M. Nanostructure Absorption: A Comparative Study of Nanowire and Colloidal Quantum Dot Absorption Cross Sections. *J. Phys. Chem. Lett.* **2010**, *1*, 3340–3348.
40. Imada, A.; Ozaki, S.; Adachi, S. Photoreflectance Spectroscopy of Wurtzite CdS. *J. Appl. Phys.* **2002**, *92*, 1793–1798.
41. Bohren, C. F.; Huffman, D. R. *Absorption and Scattering of Light by Small Particles*; Wiley-VCH: New York, 1998.